

Damped and sub-damped Lyman- α absorbers in $z > 4$ QSOs *

R. Guimarães¹, P. Petitjean², R. R. de Carvalho³, S.G. Djorgovski⁴, P. Noterdaeme⁵, S. Castro⁶, P. C. da R. Poppe¹, and A. Aghaee^{7,8}

¹ Universidade Estadual de Feira de Santana - Av. Transnordestina, s/n, 40036-900, Feira de Santana, BA - Brasil

² UPMC Paris 6, Institut d'Astrophysique de Paris, CNRS, 98bis Boulevard Arago - 75014 Paris, FRANCE

³ Instituto Nacional de Pesquisas Espaciais - INPE, Av. dos Astronautas, 1758, 12227-010, S. J. dos Campos, SP - Brasil

⁴ California Institute of Technology, MS 105-24, Pasadena, CA 91125

⁵ Inter-University Centre for Astronomy and Astrophysics, Post Bag 4, Ganeshkhind, Pune 411 007, India

⁶ European Southern Observatory, Karl-Schwarzschild Strasse, 2, Garching, Germany

⁷ Department of Physics, University of Sistan and Baluchestan, 98135 Zahedan, Iran

⁸ School of Astronomy and Astrophysics, Institute for Research in Fundamental Sciences (IPM), P.O.BOX 193595-5531, Tehran, Iran

Received 17/12/2008; accepted 07/09/2009

Abstract. We present the results of a survey for damped (DLA, $\log N(\text{H I}) > 20.3$) and sub-damped Lyman- α systems ($19.5 < \log N(\text{H I}) < 20.3$) at $z > 2.55$ along the lines-of-sight to 77 quasars with emission redshifts in the range $4 < z_{\text{em}} < 6.3$. Intermediate resolution ($R \sim 4300$) spectra have been obtained with the Echelle Spectrograph and Imager (ESI) mounted on the Keck telescope. A total of 100 systems with $\log N(\text{H I}) > 19.5$ are detected of which 40 systems are damped Lyman- α systems for an absorption length of $\Delta X = 378$. About half of the lines of sight of this homogeneous survey have never been investigated for DLAs. We study the evolution with redshift of the cosmological density of the neutral gas and find, consistently with previous studies at similar resolution, that $\Omega_{\text{DLA,H}_\text{I}}$ decreases at $z > 3.5$. The overall cosmological evolution of $\Omega_{\text{H}_\text{I}}$ shows a peak around this redshift. The H I column density distribution for $\log N(\text{H I}) \geq 20.3$ is fitted, consistently with previous surveys, with a single power-law of index $\alpha \sim -1.8 \pm 0.25$. This power-law overpredicts data at the high-end and a second, much steeper, power-law (or a gamma function) is needed. There is a flattening of the function at lower H I column densities with an index of $\alpha \sim -1.4$ for the column density range $\log N(\text{H I}) = 19.5 - 21$. The fraction of H I mass in sub-DLAs is of the order of 30%. The H I column density distribution does not evolve strongly from $z \sim 2.5$ to $z \sim 4.5$.

Key words. galaxies: evolution, galaxies: formation, quasars: absorption lines , Intergalactic Medium , cosmology: observations

1. Introduction

The amount of neutral gas in the Universe is an important ingredient of galaxy formation scenarios because the neutral phase of the intergalactic medium is the reservoir for star-formation activity in the densest places of the universe where galaxies are to be formed. It is therefore very important to make a census of the mass in this phase and to determine its cosmological evolution (see e.g. Péroux et al. 2001).

The gas with highest H I column density is detected through damped Lyman- α absorptions in the spectra of remote quasars. Although damped wings are seen for column densities of the

order of $\log N(\text{H I}) \sim 18$, the neutral phase corresponds to $\log N(\text{H I}) \geq 19.5$ (Viegas 1995). The column density defining the so-called damped Lyman- α (DLA) systems has been taken to be $\log N(\text{H I}) \geq 20.3$ because this corresponds to the critical mass surface density limit for star formation (Wolfe et al. 1986) but also because the equivalent width of the corresponding absorption is appropriate for a search of these systems in low resolution spectra. Therefore several definitions have been introduced. Ω_g^{DLA} is the mass density of baryons in DLA systems, defined arbitrarily as systems with $\log N(\text{H I}) \geq 20.3$. $\Omega_g^{\text{H}_\text{I}}$ is the mass density of neutral hydrogen in all systems : DLAs, Lyman limit systems (LLS) and the Lyman- α forest. The mass density of H I in the Lyman- α forest is negligible because the slope of the H I column density distribution is larger than -2 (~ -1.5 ; the gas is highly ionized). It is more difficult to estimate the contribution of LLS as the column density of these systems is very difficult to derive directly because the Lyman- α line lies in the logarithmic regime of the curve of growth.

Send offprint requests to: R. Guimarães, e-mail: rguimara@eso.org

* The observations reported here were obtained with the W. M. Keck Observatory, which is operated by the California Association for Research in Astronomy, a scientific partnership among the California Institute of Technology, the University of California, and the National Aeronautics and Space Administration.

However, $\Omega_g^{\text{H}_\text{I}}$ is not easily related to physical quantities as the LLS with $\log N < 19.5$ are at least partly ionized when the ones with $\log N > 19.5$ are not (see e.g. Meiring et al. 2008). On the contrary, as emphasized by Prochaska et al. (2005), hereafter PHW05, the mass density of the neutral phase, Ω_g^{neut} , is a good indicator of the mass available for star-formation and should be preferred instead. Note that Ω_g^{neut} is not equal to Ω_g^{DLA} . The column density limit at which the gas is mostly neutral cannot be defined precisely but should lie between $\log N(\text{H I}) = 19$ and 19.5. In any case, a conservative position is to consider that all systems above 19.5 are neutral.

Whether or not the mass of the neutral gas in the systems with $19.5 < \log N(\text{H I}) < 20.3$ (the so-called sub-DLAs or super-LLS) is negligible has been the source of intense discussions in recent years. Note that these discussions are related to the mass in the *neutral* phase only. Indeed, it is known for long (e.g. Petitjean et al. 1993) that the *total* mass associated with the Lyman limit systems is larger than that of DLAs. Indeed the gas in the LLS phase is mostly ionized and located in extended halos whereas DLAs are located in dense and compact regions. Péroux et al. (2003), hereafter PMSI03, have been the first to consider the sub-DLAs as an important reservoir of neutral gas. They claim that at $z > 3.5$, DLAs could contain only 50% of the neutral gas, the rest being to be found in sub-DLAs. When correcting for this, they find that the comoving mass density shows no evidence for a decrease above $z = 2$. PHW05 questioned this estimate. They use the Sloan Digital Sky Survey to measure the mass density of predominantly neutral gas Ω_g^{neut} . They find that DLAs contribute >80% of Ω_g^{neut} at all redshift. Uncertainties are very large however and the same authors estimate that the systems with $\log N(\text{H I}) > 19$ (the super-LLS) could contribute 20-50 % of $\Omega_g^{\text{H}_\text{I}}$. Therefore, the question of what is the contribution of super-LLS to Ω_g^{neut} is not settled yet.

In addition, the evolution of Ω_g^{neut} at the very high redshift, $z > 4$, is not known yet. PHW05 claim that there is no evolution of Ω_g^{DLA} for $z > 3.5$ but they caution the reader that results for $z > 4$ should be confirmed with higher resolution data. The reason is that the Lyman- α forest is so dense at these redshifts that it is very easy to misidentify a strong blend of lines with a DLA. Therefore Ω_g^{DLA} can be easily overestimated.

In this paper we present the result of a survey for DLAs and sub-DLAs at high redshift ($z > 2.55$) using intermediate resolution data. We identify a total of 100 systems with $\log N(\text{H I}) \leq 19.5$ of which 40 are DLAs over the redshift range $2.88 \leq z_{\text{abs}} \leq 4.74$ along 77 lines-of-sight towards quasars with emission redshift $4 \leq z_{\text{em}} \leq 6.3$. The sample and data reduction are presented in Section 2. In Section 3 we describe the procedures used to select the absorption systems. Section 4 analyses statistical quantities characterizing the evolution of DLAs and sub-DLAs and discusses the cosmological evolution of the neutral gas mass density. Conclusions are summarized in Section 5. Throughout the paper, we adopt $\Omega_m = 0.3$, $\Omega_\Lambda = 0.7$ and $H_0 = 72 \text{ km s}^{-1}$.

2. Observation and data reduction

Medium resolution ($R \sim 4300$) spectra of all $z > 3$ quasars discovered in the course of the DPOSS survey (Digital Palomar

Observatory Sky Survey; see, e.g., Kennefick et al. 1995, Djorgovski et al. 1999 and the complete listing of QSOs available at <http://www.astro.caltech.edu/~george/z4.qsos>) have been obtained with the Echelle Spectrograph and Imager (ESI, Sheinis et al 2002) mounted on the KECK II 10 m telescope. In total, 99 quasars have been observed, 57 of which already reported in the literature (see Table 1 for details). We provide in Table 1 a summary of the observation log for the 99 quasars. Columns 1 to 8 give, respectively, the quasar's name, the emission redshift, the apparent R magnitude, the J2000 quasar coordinates, the date of observation, the exposure time and the notes.

The echelle mode allows to cover the full wavelength range from 3900 Å to 10900 Å in ten orders with ~ 300 Å overlap between two adjacent orders. The instrument has a spectral dispersion of about $11.4 \text{ km s}^{-1} \text{ pixel}^{-1}$ and a pixel size ranging from $0.16 \text{ \AA pixel}^{-1}$ in the blue to $0.38 \text{ \AA pixel}^{-1}$ in the red. The 1 arcsec wide slit is projected onto 6.5 pixel resulting in a $R \sim 4300$ spectral resolution.

Data reduction followed standard procedures using IRAF for 70% of the sample and the programme *makee* for the remaining. For the IRAF reduction, the procedure was as follows. The images were overscan corrected for the dual-amplifier mode. Each amplifier has a different baseline value and different gain which were corrected by using a script adapted from LRIS called *esibias*. Then all the images were bias subtracted and corrected for bad pixels. The images were divided by a normalized two-dimensional flat-field image to remove individual pixel sensitivity variations. The flat-field image was normalized by fitting its intensity along the dispersion direction using a high order polynomial fit, while setting all points outside the order aperture to unity. The echelle orders were traced using the spectrum of a bright star. Cosmic rays were removed from all two-dimensional images. For each exposure the quasar spectrum was optimally extracted and background subtracted. The task *apall* in the IRAF package *echelle* was used to do this. The CuAr lamps were individually extracted using the quasar's apertures. Lines were identified in the arc lamp spectra by using the task *ecidentify* and a polynomial was fitted to the line positions resulting in a dispersion solution with a mean RMS of 0.09 Å. The dispersion solution computed on the lamp was then assigned to the object spectra by using the task *dispcor*. Wavelengths and redshifts were computed in the heliocentric restframe. The different orders of the spectra were combined using the task *scombine* in the IRAF package. It is important to note that the signal-to-noise ratio drops sharply at the edges of the orders. We have therefore carefully controlled this procedure to avoid any spurious feature.

The SNR per pixel was obtained in the regions of the Lyman- α forest that are free of absorption and the mean SNR value, averaged between the Lyman- α and Lyman- β QSO emission lines, was computed. We used only spectra with mean SNR ≥ 10 . For simplicity, we excluded from our analysis broad absorption line (BAL) quasars. We therefore used 77 lines-of-sight out of the 99 available to us.

The continuum was automatically fitted (Aracil et al. 2004; Guimarães et al. 2007) and the spectra were normalized. We checked the normalization for all lines-of-sight and manu-

ally corrected for local defects especially in the vicinity of the Lyman- α emission lines and when the Lyman- α forest is strongly blended.

Metallicities measured for twelve $z > 3$ DLAs observed along five lines-of-sight of this sample have been published by Prochaska et al. (2003b); see also Prochaska et al. (2003a).

3. Identification of Damped and sub-Damped Lyman- α systems

We used an automatic version of the Voigt profile fitting routine VPFIT (Carswell et al. 1987) to decompose the Lyman- α forest of the spectra in individual components. As usual, we restricted our search outside of 3000 km s^{-1} from the QSO emission redshift. This is to avoid contamination of the study by proximate effects such as the presence of overdensities around quasars (e.g. Rollinde et al. 2005, Guimarães et al. 2007).

From this fit we could identify the candidates with $\log N(\text{H I}) - \text{error} \geq 19.5$. We then carefully inspected each of these candidates individually with special attention to the following characteristics of DLA absorption lines:

- the wavelength range over which the line is going to zero;
- the presence of damped wings;
- the identification of associated metal lines when possible.

The redshift of the H I absorptions was adjusted carefully using the associated metal absorption features and the final H I column density was then refitted using the high order lines in the Lyman series when Lyman series are covered by our spectrum and not blended with other lines. After applying the above criteria, 100 DLAs and sub-DLAs with $\log N(\text{H I}) \geq 19.5$ were confirmed. A total of 65 systems were not previously used for $\Omega_{\text{DLA},\text{H}_\text{I}}/\Omega_{\text{sub-DLA},\text{H}_\text{I}}$ estimations, 21 of which are DLAs and 44 are sub-DLAs. Their characteristics are given in Table 2: Columns 1 to 7 give, respectively, the QSO's name; the emission redshift estimated as the average of the determinations from the peak of the Ly α emission and from the peak of a Gaussian fitted to the CIV emission line; the minimum redshift along a DLA/sub-DLA could be detected; the maximum redshift along a DLA/sub-DLA could be detected; the redshift of the DLA/sub-DLA; the DLA/sub-DLA H I column density; associated detected metal lines and notes. Lyman series and selected associated metal lines are shown in the Appendix "List of Figures". The QSO lines of sight of our sample along which we detect no DLA and/or sub-DLA are listed in Table 3. Comments on DLA/sub-DLA systems differences between our measurements and measurements by others are in the Appendix "Notes on Individual Systems".

The metal lines have been searched for using a search list of the strongest atomic transitions given in Table 4. The corresponding absorptions have been fitted using the package VPFIT. A full account of this metallic column densities and the corresponding abundances is out of the scope of this paper and will be presented elsewhere (Guimarães et al., in preparation).

4. Analysis

Using the procedure described in the previous Section, we detect 100 systems with $\log N(\text{H I}) \geq 19.5$, out of which 40 are DLAs. We use this sample to investigate the characteristics of the neutral phase over the redshift range $2.5 \leq z \leq 5$. We compare in Fig 1 the redshift sensitivity function of our survey with the redshift sensitivity function of previous surveys computed by PMSI03. Although the redshift path of our survey is much

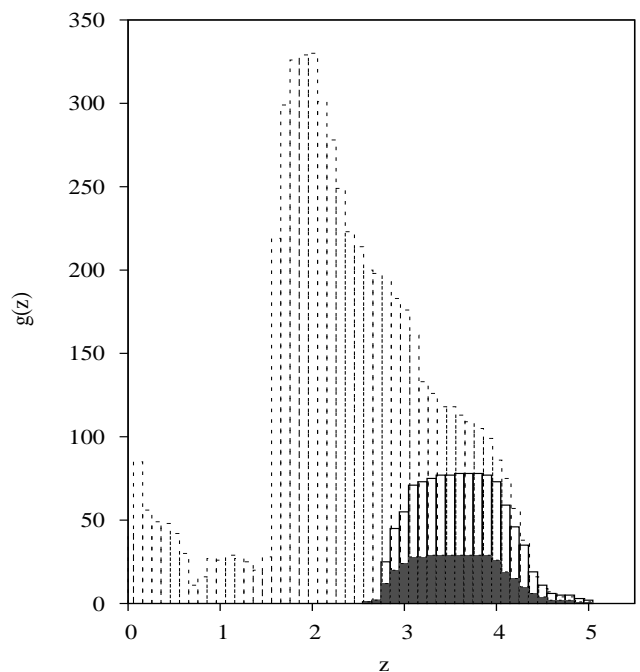


Fig. 1. Solid curve shows the redshift sensitivity function of our survey for all lines-of-sight, the filled grey histogram is only for unpublished lines-of-sight. Dashed curve shows the redshift sensitivity function of previous surveys computed by PMSI03.

smaller than that of the SDSS survey (PHW05), it is at $z > 3.5$ similar to the surveys by Péroux et al. (2001, 2003). Note that our survey is homogeneous and at spectral resolution twice or more larger than previous surveys. The H I column density distribution of the 100 DLAs and sub-DLAs measured in this work and that of the systems with $\log N(\text{H I}) \geq 20.3$ in PMSI03 are shown in Fig. 2. We are confident that we do not miss a large number of sub-DLAs down to the above limit.

To give a global overview of the survey, we plot in Fig. 3, $\log N(\text{H I})$ versus z_{abs} for the 65 unpublished damped/sub-DLA absorption systems. In the same figure we show for comparison the data points from the Péroux et al. (2001) survey.

In Figure 4, we plot for comparison, as a function of redshift, the difference between the H I column densities measured for the same systems by us and by either Péroux et al. (2005) from high-resolution data or Prochaska & Wolfe (2009) from SDSS data. The measurements are consistent within errors.

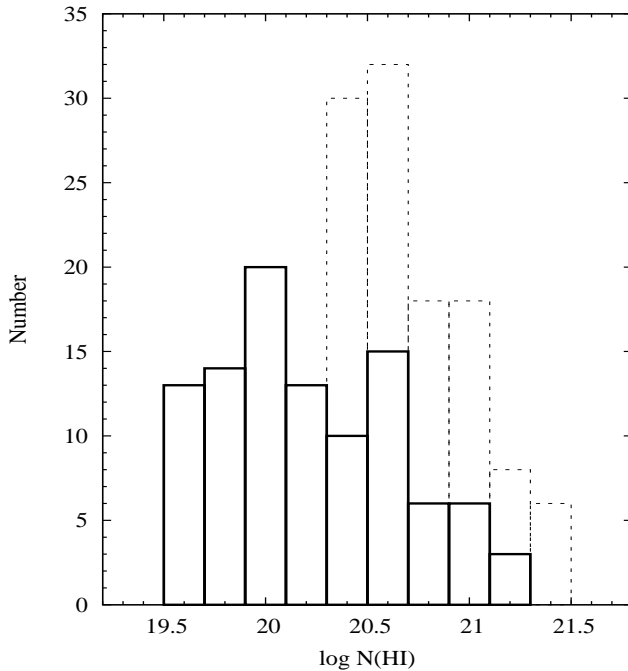


Fig. 2. Histogram of the H I column densities measured for the 100 DLAs and sub-DLAs with $\log N(\text{H I}) \geq 19.5$ detected in our survey (solid-line histogram). The dashed-line histogram represents the H I column densities measured by PMSI03 with $\log N(\text{H I}) \geq 20.3$.

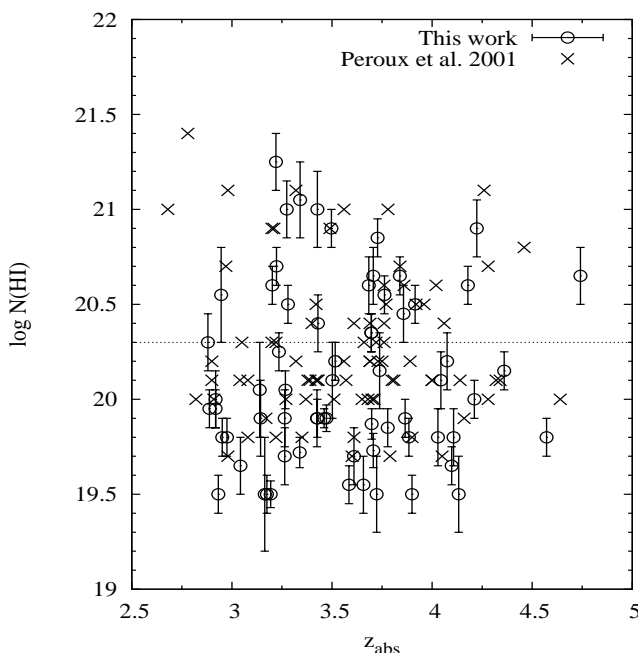


Fig. 3. The logarithm of the H I column density measured in our unpublished systems (circles) is plotted versus the redshift. The data points of Péroux et al. (2001) are shown for comparison with crosses.

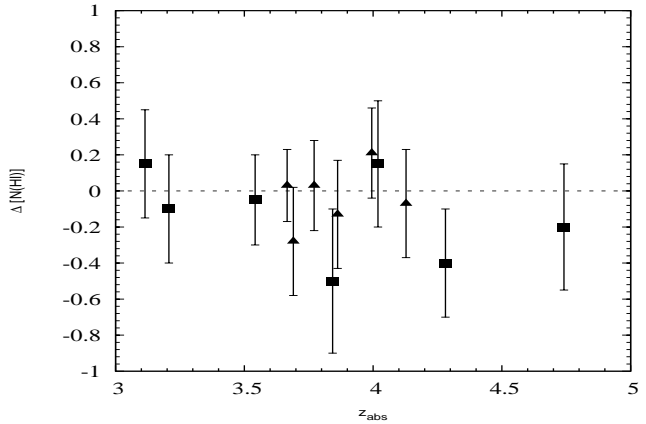


Fig. 4. The H I column density difference between our measurements and those by either Péroux et al. (2005) (triangles) or Prochaska & Wolfe (2009) (squares) in systems common to different surveys is plotted versus redshift.

4.1. Column Density Distribution Function

The H I absorption system frequency distribution function is defined as:

$$f(N, X)dN dX = \frac{m_{\text{sys}}}{\Delta N \times \sum_i^n \Delta X_i} dN dX \quad (1)$$

where m_{sys} is the number of absorption systems with a column density comprised between $N - \Delta N/2$ and $N + \Delta N/2$ and observed over an absorption distance interval of ΔX . The total absorption distance coverage, $\sum_i^n \Delta X_i$, is computed over the whole sample of n QSO lines-of-sight. The absorption distance, X , is defined as

$$X(z) = \int_0^z (1+z)^2 E(z) dz \quad (2)$$

where $E(z) = [\Omega_M(1+z)^3 + \Omega_\Lambda]^{-1/2}$. For one line-of-sight, $\Delta X(z) = X(z_{\text{max}}) - X(z_{\text{min}})$, with z_{max} being the emission redshift minus 3000 km s^{-1} and z_{min} is the redshift of an H I Lyman- β line located at the position of the QSO Lyman- β emission line. In Figure 5 we show the function $f(N, X)$ obtained from our statistical sample over the redshift range $z = 2.55 - 5.03$ and for $\log N(\text{H I}) \geq 19.5$. It can be seen that there is no break at the low column density end, between $\log N(\text{H I}) = 19.5$ and 20.6. This makes us confident that we are complete down to $\log N(\text{H I}) = 19.5$. The vertical bars indicate 1σ errors. The horizontal bars indicate the bin sizes plotted at the mean column density for each bin. PHW05 results in the redshift range

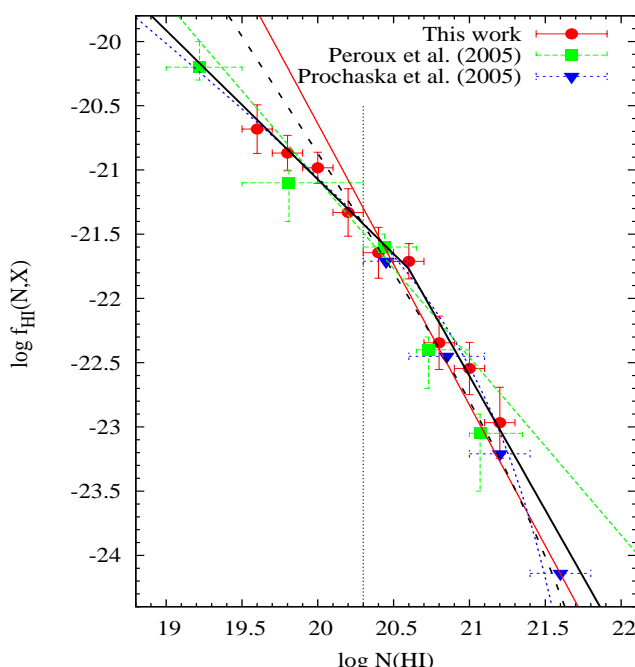


Fig. 5. Frequency distribution function over the redshift range $z = 2.55 - 5.03$. The dashed green, solid black and dotted blue lines are, respectively, a power-law, a double power-law and a gamma function fits to the data. The solid red and dashed black lines are, respectively, a power-law and gamma function fits to the data obtained by PHW05.

$z = 2.2 - 5.5$ and for $\log N(\text{H I}) \geq 20.3$ are overplotted in the same figure. Although our data points are consistent within about 1σ with those of PHW05, it seems that the overwhole shape of the function is flatter in our data. Note that we do not detect any system with $\log N(\text{H I}) > 21.25$. Data points from Péroux et al. (2005), hereafter PDDKM05, are also overplotted. Our point at $\log N(\text{H I}) = 19.5$ is consistent with theirs.

A power-law, a gamma function and/or a double power-law are usually used to fit the frequency distribution. It is apparent from Fig. 5 that a power-law (of the form $f(N, X) = K \times N^{-\alpha}$) fits the function nicely over the column density range $19.5 < \log N(\text{H I}) < 21$. The index of this power spectrum (see Table 5) is larger ($\alpha \sim -1.4$) than what is found by PHW05 but over a smaller column density range $\log N(\text{H I}) > 20.3$. The discrepancy is apparently due to the difference in the column density ranges considered by both studies. If we restrict our fit to the same range as PHW05 we find an index of $\alpha \sim -1.8 \pm 0.25$ which is consistent with the results of PHW05. We note that PDDKM05 already mentioned that the small end of the column density distribution is flatter than $\alpha = -2$.

There is a large deficit of high column density systems in our survey compared to what would be expected from the single power-law fit. This has been noted before and discussed in detail by PHW05. A double power-law was used to fit our full sample with better result (see Table 5). However, the sharp break in the function at $\log N(\text{H I}) \sim 21$ suggests a gamma func-

tion of the form, $f(N, X) = K \times (\frac{N}{N_T})^{-\alpha} \times e^{\frac{-N}{N_T}}$ (Pei & Fall 1995) should better describe the data.

We have calculated the frequency distribution function, $f(N, X)$, in different redshift bins of equal distance path : 2.55–3.40; 3.40–3.83 and 3.83–5.03. Results are shown in Fig. 6. The functions are fitted as described above and fit results are given in Table 5. We find that the function do not evolve much with redshift. This is consistent with the finding by PHW05 that the global characteristics of the function are not changing much with time. There is however a tendency for a flattening of the function which may indicate that the number of sub-DLAs relatively to other systems is larger at lower redshift. Although we do not think this is the case because we have used a conservative approach, part of this evolution at the highest redshift could possibly be a consequence of loosing the sub-DLAs in the strongly blended Lyman- α forest at $z > 4$. We note also a slight decrease of the number of systems with $\log N(\text{H I}) > 20.5$ at the highest redshifts. This is consistent with the finding by PDDKM05 that the relative number of high column density DLAs decreases with redshift.

Another way to look at these variations is to compute the redshift evolution of the number of (sub)DLAs per unit path length. The observed density of systems is defined as

$$l_{(\text{sub})\text{DLAs}} = \int_{N_{\min}}^{N_{\max}} f(N, X) dN \quad (3)$$

Results obtained during the present survey together with those of PHW05 and PDDKM05 are plotted in Figure 7. The important feature of this plot is that the number density of DLAs peaks at $z \sim 3.5$. In addition, the ratio of the number of sub-DLAs to the number of DLAs is larger at redshift < 3.5 compared to higher redshifts.

4.2. Neutral hydrogen cosmological mass density, Ω_{H_1}

The comoving mass density of neutral gas is given by

$$\Omega_{\text{H}_1}(z) = \frac{H_0}{c} \frac{\mu m_{\text{H}}}{\rho_0} \frac{\Sigma_i N_i(\text{H}_1)}{\Delta X(z)} \quad (4)$$

where the density is in units of the current critical density ρ_0 ; m_{H} is the mass of the hydrogen atom, $\mu = 1.3$ is the mean molecular weight, ΔX the absorption length and the summation of column densities is done over all absorption systems detected in the survey. Results are shown in Fig. 8 and summarized in Table 6. The three redshift bins considered are defined so that the absorption length is equal in each bin. The different columns of Table 6 give, respectively, the redshift range, the mean redshift, the number of lines-of-sight involved, the number of DLAs and sub-DLAs detected over this redshift range, the absorption length (calculated using z_{\min} and z_{\max} as defined in Table 2), the resulting H_1 cosmological densities for, respectively, DLAs only or both DLAs and sub-DLAs.

Results from PHW05 and PDDKM05 are also plotted on Figure 8. It can be seen that we confirm the decrease of Ω_{H_1} for $z > 3$ that was noticed by PDDKM05. The measurement from the SDSS in this redshift range is higher. However, our survey is of higher spectral resolution and should in principle be more

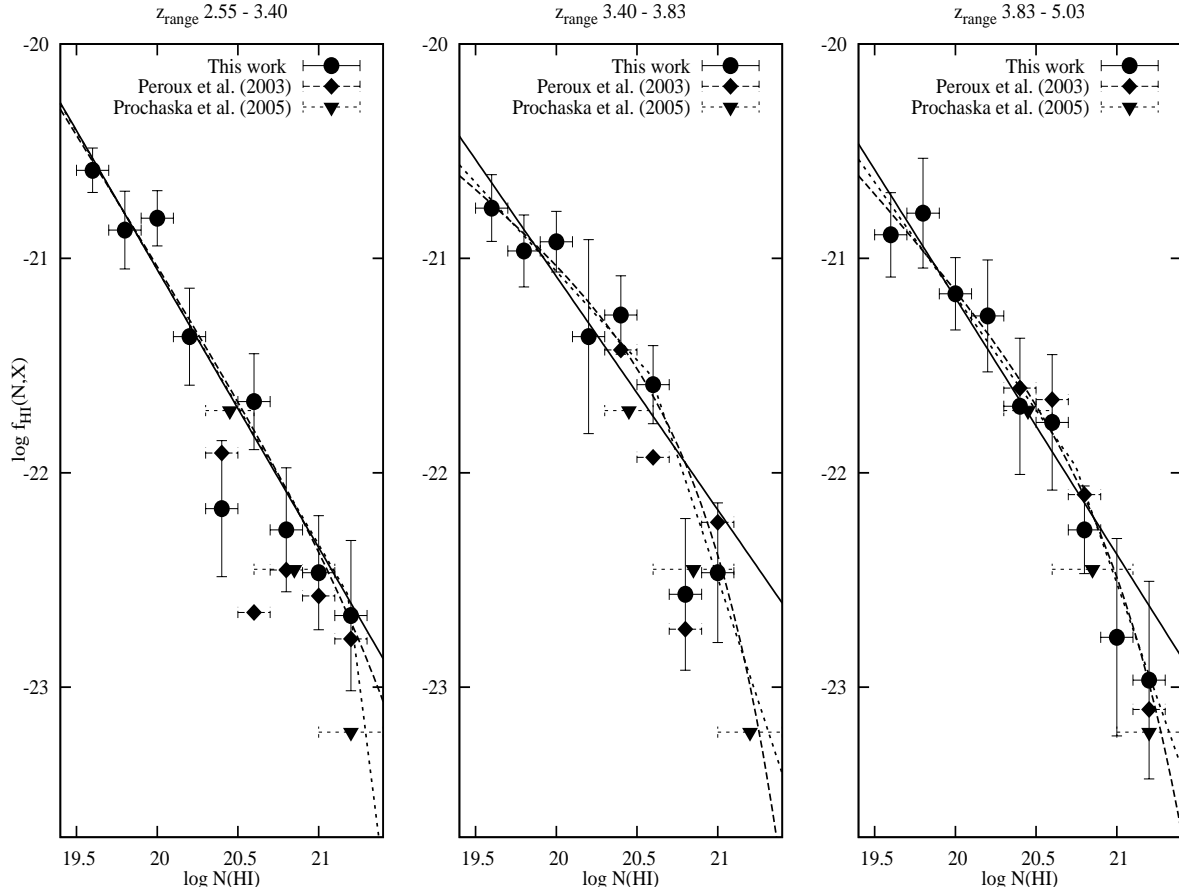


Fig. 6. H I frequency distribution, $f_{\text{HI}}(N, X)$, in three redshift bins: 2.55–3.40 (left), 3.40–3.83 (center), and 3.83–5.03 (right). Straight lines show best χ^2 fits of a power-law function to the binned data. The dashed curve is the same for a gamma function fit, and the dot-dashed curve for a double power-law fit.

reliable in this redshift range. It seems that the evolution of Ω_{H_1} is a steep increase from $z = 2$ to $z = 3$ and then a slightly flatter decrease up to $z = 5$. The inclusion of the sub-DLAs does not change this picture as sub-DLAs contribute to a maximum of about 30% to the total H I mass. The contribution by sub-DLAs is better seen in Fig. 9 where we plot the cumulative density versus the maximum H I column density considered. As noted already by numerous authors, the discrepancy of measurements at $z < 1.5$ is still a problem.

It can be also seen from the Figure 8 that Ω_{H_1} are lower than Ω_{stellar} , the mass density in stars in local galaxies. We find for the ratio of the peak value of Ω_{H_1} to Ω_{stellar} for this work $R \sim 0.45$. Previous surveys, PDDKM05 and PHW05, have found for the ratio 0.37 and 0.40 respectively.

5. Discussion

We have presented the results of a survey for damped and sub-damped Lyman- α systems ($\log N(\text{H I}) \geq 19.5$) at $z \geq 2.55$ along the lines-of-sight to 77 quasars with emission redshifts in the range $4 \geq z_{\text{em}} \geq 6.3$. In total 99 quasars were observed but 22 lines-of-sight were not used because of not enough SNR and/or because of the presence of broad absorption lines.

Intermediate resolution ($R \sim 4300$) spectra have been obtained with the Echelle Spectrograph and Imager (ESI) mounted on the Keck telescope. The damped Lyman- α absorptions are identified on the basis of (i) the width of the saturated absorption, (ii) the presence of damped wings and (iii) the presence of metals at the corresponding redshift. The detection is run automatically but all lines are verified visually. A total of 100 systems with $\log N(\text{H I}) \geq 19.5$ are detected of which 40 systems are Damped Lyman- α systems ($\log N(\text{H I}) \geq 20.3$) for an absorption length of $\Delta X = 378$. Spectra are shown in Appendix.

PHW05 have derived from SDSS data that the cosmological density of the neutral gas increases strongly by a factor close to two from $z \sim 2$ to $z \sim 3.5$. Beyond this redshift, measurements are more difficult because the Lyman- α forest is dense. Our measurements should be more reliable because of better spectral resolution. We show, consistently with the findings of PDDKM05, that the cosmological density of the neutral gas decreases at $z > 3.5$. The overall cosmological evolution seems therefore to have a peak at this redshift.

We find that the H I column density distribution does not evolve strongly from $z \sim 2.5$ to $z \sim 4$. The one power-law fit in the range $\log N(\text{H I}) > 20.3$ gives an index of $\alpha = -1.80 \pm 0.25$, consistent with previous determinations. However, we find that

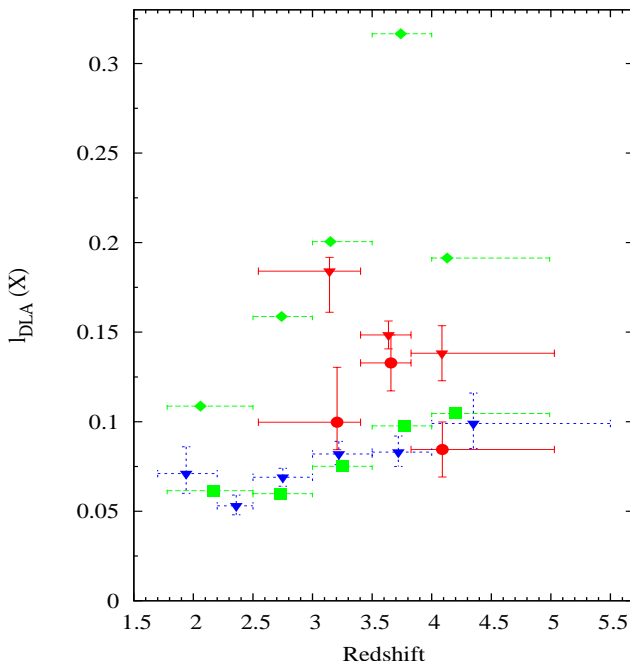


Fig. 7. Number density of absorbers vs. redshift. Red circles and inverse triangles are from this work for DLAs and sub-DLAs, respectively. The values obtained by PWH05 (blue inverse triangles) and PDDKM05 (green squares) for DLAs are overplotted. The green diamonds are the values obtained for $\log N(\text{H I}) > 19.0$ by PDDKM05.

the fit over the column density range $\log N(\text{H I}) = 19.5\text{--}21$ is quite flat ($\alpha \sim 1.4$). This probably indicates that the slope at the low-end is much flatter than -2 . This power-law overpredicts data at the high-end and a second much steeper power-law (or a gamma function) is needed. The fraction of H I mass in sub-DLAs is of the order of 30%. Our data do not support the claim by PDDKM05 that the incidence of low column-density systems is larger at high redshift. The number density of sub-DLAs seems to peak at $z \sim 3.5$ as well.

It is apparent that statistical errors are still large in our survey. It would be therefore of first importance to enlarge the sample of (sub)DLAs at high redshift. For this we need to go to fainter quasars however. The advent of X-shooter, a new generation spectrograph at the VLT with a spectral resolution of $R = 6700$ in the optical, should allow this to be done in a reasonable amount of observing time.

Acknowledgements. SGD is supported by the NSF grant AST-0407448, and the Ajax Foundation. Cataloguing of DPOSS and discovery of PSS QSOs was supported by the Norris Foundation and other private donors. We thank E. Thiébaut, and D. Munro for freely distributing his yorick programming language (available at <ftp://ftp-icf.llnl.gov/pub/Yorick>), which we used to implement our analysis. The authors wish to recognize and acknowledge the very significant cultural role and reverence that the summit of Mauna Kea has always had within the indigenous Hawaiian community. We are most fortunate to have the opportunity to conduct observations from this mountain. We acknowledge the Keck support staff for their efforts in performing these observations.

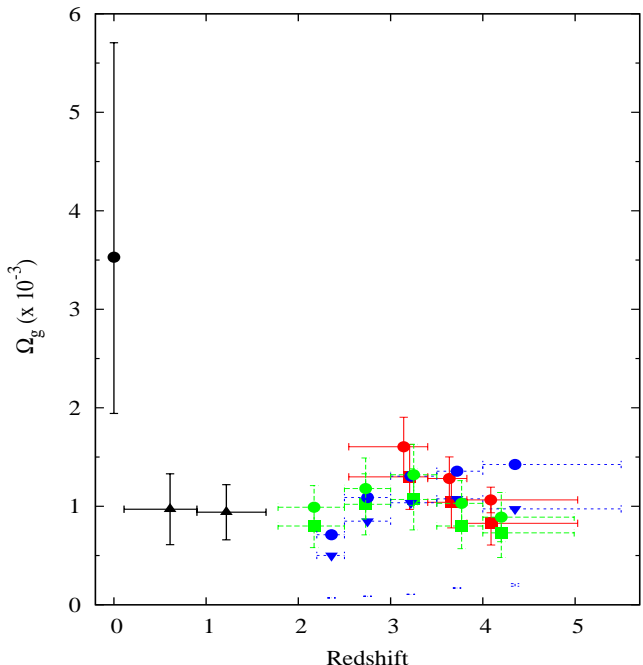


Fig. 8. Cosmological evolution of the H I mass density. For DLAs: red squares are the results of this work, green squares are from PDDKM05, blue inverse triangles from PHW05 and black triangles from Rao et al. (2005). For sub-DLAs: red circles are this work (for systems with column densities ≥ 19.5), green circles obtained from PDDKM05 (for systems with column densities ≥ 19.0) and blue circles obtained from PHW05 (as determined from the single power-law fit to the LLS frequency distribution function). The black circle are the mass density in stars in local galaxies (Fukugita et al. 1998).

References

- Aracil, B., Petitjean, P., Pichon, C., & Bergeron, J. 2004, A&A, 419, 811
- Carswell, R. F., Webb, J. K., Baldwin, J. A., & Atwood, B. 1987, ApJ, 319, 709
- Dessauges-Zavadsky, M., Péroux, C., Kim, T.-S., D'Odorico, S., & McMahon, R. G. 2003, MNRAS, 345, 447
- Djorgovski, S. G., Odewahn, S. C., Gal, R. R., Brunner, R. J., & de Carvalho, R. R. 1999, in Weymann R. J., Storrie-Lombardi L. J., Sawicki M., Brunner R. J., eds, ASP Conf. Ser. Vol. 191, Photometric Redshifts and the Detection of High Redshift Galaxies. Astron. Soc. Pac., San Francisco, p. 179
- Fukugita, M., Hogan, C. J. & Peebles, P. J. E. 1998, ApJ, 503, 518
- Guimarães, R., Petitjean, P., Rollinde, E., de Carvalho, R. R., Djorgovski, S. G., Srianand, R., Aghaei, A., & Castro, S. 2007, MNRAS, 377, 657
- Kennefick, J. D., Djorgovski, S. G., & de Carvalho, R. R. 1995, AJ, 110, 2553
- Meiring, J. D., Kulkarni, V. P., Lauroesch, J. T., Péroux, C., Khare, P., York, D. G., & Croots, A. P. S. 2008, MNRAS, 384, 1015
- Pei, Y. C., & Fall, S. M. 1995, ApJ, 454, 69
- Péroux, C., Storrie-Lombardi, L. J., McMahon, R. G., Irwin, M., & Hook, I. M. 2001, AJ, 121, 1799
- Péroux, C., McMahon, R. G., Storrie-Lombardi, L. J., & Irwin, M. J. 2003, MNRAS, 346, 1103 (PM03)

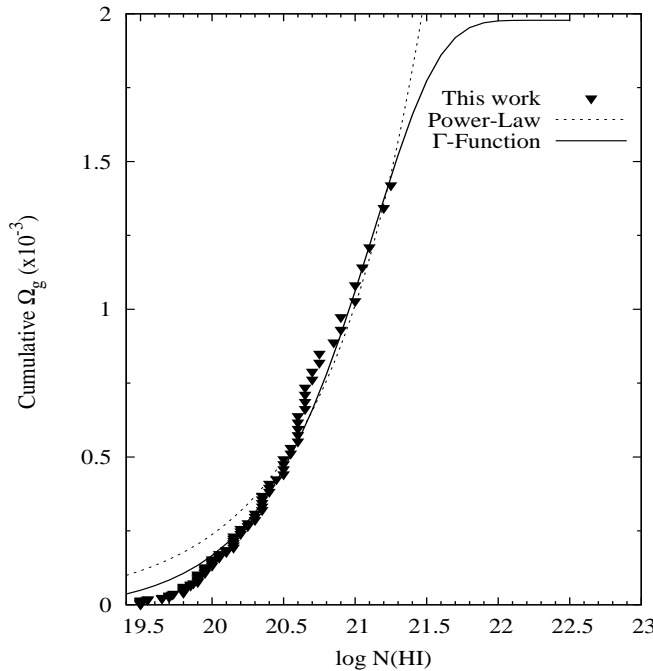


Fig. 9. Ω_{HI} is plotted as a function of the maximum $\log N(\text{H I})$ considered

- Péroux, C., Dessauges-Zavadsky, M., D’Odorico, S., Sun Kim, T., & McMahon, R. G. 2005, MNRAS, 363, 479 (PDDKM05)
 Petitjean, P., Webb, J. K., Rauch, M., Carswell, R. F., & Lanzetta, K. 1993, MNRAS, 262, 499
 Prochaska, J. X., Castro, S., & Djorgovski, S. G. 2003, ApJS, 148, 317
 Prochaska, J. X., Gawiser, E., Wolfe, A. M., Castro, S., & Djorgovski, S. G. 2003, ApJ, 595, L9
 Prochaska, J. X., Herbert-Fort, S., & Wolfe, A. M. 2005, ApJ, 635, 123 (PHW05)
 Prochaska, J. X., & Wolfe, A. M. 2009, ApJ, 696, 1543
 Rao, S. M., Turnshek, D. A., & Nestor, D. B. 2006, ApJ, 636, 610
 Rollinde, E., Srianand, R., Theuns, T., Petitjean, P., & Chand, H. 2005, MNRAS, 361, 1015
 Sheinis, A. I., Bolte, M., Epps, H. W., Kibrick, R. I., Miller, J. S., Radovan, M. V., Bigelow, B. C., & Sutin, B. M. 2002, PASP, 114, 851
 Storrie-Lombardi, L. J., & Wolfe, A. M. 2000, ApJ, 543, 552
 Viegas, S. M. 1995, MNRAS, 276, 268
 Wolfe, A. M., Turnshek, D. A., Smith, H. E., & Cohen, R. D. 1986, ApJS, 61, 249

Table 1. Summary of Observations

QSO	z_{em}	R	RA(2000)	DEC(2000)	Obs. Date	Exp. Time (min)	Note*
PSS0007+2417	4.050	18.69	00 07 38.7	+24 17 25.0	2000 Sep 06	60	
PSS0014+3032	4.470	18.81	00 14 42.8	+30 32 03.0	2000 Sep 06	60	
PSS0052+2405	4.280	18.30	00 52 06.8	+24 05 39.0	1999 Dec 30	40	
PSS0117+1552	4.244	18.60	01 17 31.2	+15 52 16.4	2000 Sep 04	50	2
PSS0118+0320	4.232	18.50	01 18 52.8	+03 20 50.0	2000 Sep 06	60	3
PSS0121+0347	4.127	17.86	01 21 26.2	+03 47 07.0	1999 Dec 30	45	3
SDSS0127-0045	4.084	18.37	01 27 00.7	-00 45 59.4	2001 Jan 02	60	
PSS0131+0633	4.430	18.24	01 31 12.2	+06 33 40.0	2000 Sep 04	60	1, 2
PSS0133+0400	4.154	17.86	01 33 40.4	+04 00 59.0	1999 Dec 29	40	1, 2, 3
PSS0134+3307	4.536	18.82	01 34 21.6	+33 07 56.5	2000 Sep 06	60	1, 2
PSS0207+0940	4.136	18.63	02 07 03.5	+09 40 59.0	2000 Sep 04	75	
SDSS0206+1216	4.810	21.51	02 06 51.4	+12 16 24.4	2002 Dec 07	30	
PSS0209+0517	4.194	17.36	02 09 44.7	+05 17 14.0	1999 Dec 29	35	1, 2, 3
SDSS0210-0018	4.700	20.74	02 10 43.2	-00 18 18.5	2002 Dec 07	40	4, 5
PSS0211+1107	3.975	18.12	02 11 20.1	+11 07 16.0	1999 Dec 29	70	
SDSS0211-0009	4.900	22.04	02 11 02.7	-00 09 10.3	2002 Dec 07	20	1, 2
SDSS0231-0728	5.410	21.54	02 31 37.6	-07 28 54.5	2002 Dec 06	90	4, 5
PSS0244-0108	3.990	19.00	02 44 57.2	-01 08 08.7	2000 Sep 06	40	4, 5
PSS0248+1802	4.422	18.40	02 48 54.3	+18 02 50.3	1999 Dec 30	60	1, 2
PSS0320+0208	3.960	18.74	03 20 42.7	+02 08 16.0	1999 Dec 30	55	
SDSS0338+0021	5.020	21.68	03 38 29.3	+00 21 56.5	2002 Dec 06	90	1, 2, 4, 5
SDSS0338-RD657	4.960	23.00	03 38 31.3	+00 18 07.7	2001 Jan 02	120	
PSS0452+0355	4.420	18.80	04 52 51.5	+03 55 58.0	1999 Dec 30	60	
PSS0747+4434	4.435	18.06	07 47 50.0	+44 34 16.0	1999 Dec 30	90	1, 2, 5
SDSS0756+4104	5.090	21.70	07 56 18.0	+41 04 10.6	2001 Mar 26	150	4
PSS0808+5215	4.510	18.82	08 08 49.5	+52 15 16.0	2000 Apr 28	70	5
SDSS0810+4603	4.074	18.67	08 10 54.7	+46 03 55.2	2001 Mar 24	60	
PSS0852+5045	4.200	19.00	08 52 27.4	+50 45 11.0	2000 May 13	60	
PSS0926+3055	4.190	17.31	09 26 36.3	+30 55 06.0	1999 Dec 29	40	
SDSS0941+5947	4.820	20.66	09 41 08.4	+59 47 25.8	2002 Dec 06	40	4, 5
BR0945-0411	4.130	18.80	09 47 49.6	-04 25 15.1	2000 May 14	60	
PSS0950+5801	3.973	17.38	09 50 14.0	+58 01 38.0	1999 Dec 29	40	4, 5
BR0951-0450	4.350	18.90	09 53 55.7	-05 04 19.5	2000 May 15	53	2
PSS0955+5940	4.340	17.84	09 55 11.3	+59 40 32.0	1999 Dec 29	56	4, 5
PSS0957+3308	4.283	17.59	09 57 44.5	+33 08 23.0	1999 Dec 29	55	5
BRI1013+0035	4.380	18.80	10 15 49.0	+00 20 19.0	2000 May 15	60	2
PSS1026+3828	4.180	18.93	10 26 56.7	+38 28 43.0	2000 Apr 29	95	5
BR1033-0327	4.509	18.50	10 36 23.7	-03 43 20.0	2000 May 13	20	
PSS1039+3445	4.390	19.20	10 39 19.3	+34 45 10.9	2001 Apr 18	150	5
SDSS1044-0125	5.740	25.10	10 44 33.0	-01 25 03.1	2000 Apr 28 & 2001 Jan 01,02	330	
SDSS1048+4637	6.230	22.40	10 48 45.0	+46 37 18.3	2003 Jun 02	90	5
PSS1048+4407	4.450	19.50	10 48 46.6	+44 07 12.7	2000 Apr 29	20	
PSS1057+4555	4.126	17.70	10 57 56.4	+45 55 51.9	1999 Dec 30	40	1, 2, 5
PSS1058+1245	4.330	18.00	10 58 58.5	+12 45 55.0	1999 Dec 30	75	
PSS1118+3702	4.030	18.76	11 18 56.2	+37 02 53.9	2001 Mar 24	60	5
PSS1140+6205	4.509	18.73	11 40 09.6	+62 05 23.3	2000 May 14	60	4, 5
PSS1159+1337	4.081	18.50	11 59 06.5	+13 37 37.8	2000 Feb 10	55	1, 2, 5
SDSS1204-0021	5.030	20.82	12 04 41.7	-00 21 49.6	2003 Jun 04	60	4, 5
SDSS1208+0010	5.273	22.75	12 08 23.9	+00 10 28.9	2001 Mar 24	120	
PSS1226+0950	4.340	18.78	12 26 23.8	+09 50 03.7	2001 Mar 24	80	
PSS1247+3406	4.897	20.40	12 49 42.2	+33 49 54.0	2001 Mar 26	60	
PSS1248+3110	4.346	18.90	12 48 20.2	+31 10 44.0	2000 May 13	60	
PSS1253-0228	4.007	19.40	12 53 36.3	-02 28 08.0	2000 Apr 29	55	1,2
SDSS1310-0055	4.151	18.85	13 10 52.6	-00 55 31.8	2001 Mar 24	50	4, 5

Table 1. continued.

QSO	z_{em}	R	RA(2000)	DEC(2000)	Obs. Date	Exp. Time (min)	Note*
PSS1315+2924	4.180	18.48	13 15 39.6	+29 24 39.8	2001 Mar 24	85	
PSS1317+3531	4.369	19.10	13 17 43.3	+35 31 33.1	2001 Mar 26	55	2
J1325+1123	4.400	18.77	13 25 12.6	+11 23 32.8	2001 Apr 18	120	5
PSS1326+0743	4.123	17.30	13 26 11.9	+07 43 59.0	2000 Dec 29	60	
PSS1339+5154	4.080	18.70	13 39 13.0	+51 54 04.0	2000 May 15	60	5
PSS1347+4956	4.560	17.90	13 47 43.4	+49 56 21.0	2000 Feb 10	50	5
PSS1401+4111	4.026	18.62	14 01 32.8	+41 11 49.9	2000 Apr 28	46	4, 5
PSS1403+4126	3.862	18.92	14 03 55.7	+41 26 16.2	2000 May 15	90	4, 5
PSS1418+4449	4.280	18.40	14 18 31.8	+44 49 37.0	2000 Feb 29	60	4, 5
PSS1430+2828	4.306	19.30	14 30 31.9	+28 28 34.1	2001 Mar 26	55	2
PSS1432+3940	4.292	18.60	14 32 24.9	+39 40 24.0	2000 May 13	60	4, 5
PSS1435+3057	4.350	19.30	14 35 23.3	+30 57 16.3	2001 Apr 18	70	2
PSS1443+2724	4.406	19.30	14 43 31.2	+27 24 37.0	2000 Apr 29	30	2
PSS1443+5856	4.270	17.80	14 43 40.8	+58 56 53.0	2000 Apr 28	40	4, 5
PSS1458+6813	4.291	18.67	14 58 31.7	+68 13 05.2	2000 Apr 28	60	
PSS1500+5829	4.224	18.60	15 00 07.7	+58 29 38.0	2000 May 14	60	
PSS1506+5220	4.180	18.10	15 06 54.6	+52 20 05.0	2000 Feb 10	50	4, 5
GB1508+5714	4.304	18.90	15 10 02.2	+57 03 04.9	2000 May 13	75	2
PSS1531+4157	4.200	19.00	15 31 29.4	+45 17 07.9	2001 Apr 18	128	
PSS1535+2943	3.972	18.90	15 35 53.9	+29 43 13.0	2000 May 15 & 2000 Sep 05	120	
PSS1543+3417	4.390	18.40	15 43 40.4	+34 17 45.0	2000 Apr 30	76	5
PSS1554+1835	3.990	18.90	15 35 53.9	+29 43 13.0	2000 May 15 & 2000 Sep 04	120	
PSS1555+2003	4.228	18.90	15 55 02.6	+20 03 25.0	2000 May 14	90	
PSS1615+1803	4.010	18.42	16 15 22.9	+18 03 56.4	2000 Apr 29	90	
SDSS1630+4012	6.050	20.42	16 30 33.9	+40 12 09.6	2003 Jun 02,03,04	295	
PSS1633+1411	4.349	19.00	16 33 19.7	+14 11 42.6	2000 Apr 30	60	1, 2
PSS1646+5514	4.084	18.11	16 46 56.3	+55 14 46.7	2000 Apr 28	60	1, 2
VLA1713+4218	4.230	19.00	17 13 56.2	+42 18 08.6	2001 Apr 17	90	
PSS1715+3809	4.520	18.56	17 15 39.5	+38 09 06.6	2000 Sep 03	60	
PSS1721+3256	4.040	19.23	17 21 06.7	+32 56 35.8	2000 May 01	60	1, 2
PSS1723+2243	4.514	18.17	17 23 23.1	+22 43 56.4	2001 Mar 24	40	
SDSS1737+5828	4.940	20.93	17 37 44.0	+58 28 25.4	2001 Mar 24	90	4, 5
PSS1745+6846	4.130	19.12	17 45 50.1	+68 46 21.0	2000 May 01	120	
PSS1802+5616	4.158	19.19	18 02 48.9	+56 16 51.0	2000 Sep 05	90	1, 2
PSS2122-0014	4.114	19.13	21 22 07.5	-00 14 45.0	2000 Sep 06	60	1, 2, 4, 5
PSS2154+0335	4.360	18.41	21 54 06.9	+03 35 40.0	2000 May 14	60	1, 2, 3
PSS2155+1358	4.256	18.50	21 55 02.1	+13 58 26.0	2000 May 15	40	1, 2, 3
PSS2203+1824	4.375	18.74	22 03 43.4	+18 28 14.0	2000 Sep 04	60	
PSS2238+2603	4.031	18.85	22 38 41.1	+26 03 46.0	2000 Sep 06	60	
PSS2241+1352	4.441	18.69	22 41 47.7	+13 52 05.9	2000 Sep 03	60	1, 2, 4, 5
PSS2244+1005	4.040	18.92	22 44 05.5	+10 47 38.0	2000 Sep 04	80	
PSS2315+0921	4.412	18.96	23 15 59.2	+09 21 44.0	2000 Sep 05	90	
PSS2322+1944	4.170	18.29	23 22 07.2	+19 44 23.0	2000 May 13 & 2000 Sep 04	111	
PSS2323+2758	4.180	18.51	23 23 41.0	+27 58 01.0	2000 Sep 04	86	
PSS2344+0342	4.340	17.87	23 44 03.2	+03 42 26.0	1999 Dec 30	45	1, 2

* Quasars from this survey were previously used for $\Omega_{\text{DLA,HI}}$ estimations by: (1) Péroux et al. (2001); (2) Péroux et al. (2003); (3) Péroux et al. (2005); (4) Prochaska et al. (2005); (5) Prochaska & Wolfe (2009)

Table 2. List of DLA-subDLAs

QSO	z_{em}	z_{min}	z_{max}	DLA-subDLA		Metal Lines	Note [*]
				z_{abs}	$\log N(\text{H I})$		
PSS0007+2417	4.05	2.758	4.000	3.194	19.50±0.07	Si II, C IV	
				3.497	20.95±0.10	Si II, Fe II, Al II	
				3.706	20.65±0.15	Si II, O I, C II, Si IV, C IV, Fe II, Al II	
				3.839	20.65±0.10	Si II, O I, C II, C IV, Fe II, Al II	
PSS0117+1552	4.244	2.784	4.192	3.175	19.50±0.10	C IV	
PSS0118+0320	4.232	2.901	4.180	4.128	19.95±0.15	Si II, O I, C II, Si IV, C IV, Al II	3
PSS0121+0347	4.127	2.789	4.076	2.977	19.50±0.15	no metals ^a	3
SDSS0127-0045	4.084	2.546	4.033	3.728	20.85±0.10	Si II, O I, C II, Si IV, C IV, Fe II, Al II	
PSS0131+0633	4.430	3.008	4.376	3.173	19.95±0.10	Fe II, Al II	1, 2
				3.689	19.50±0.10	C IV	1, 2
				3.995	20.15±0.10	O I, C II, Si IV, C IV, Fe II	3
PSS0133+0400	4.154	2.930	4.102	3.690	20.40±0.15	Si II	1, 2, 3
				3.771	20.45±0.15	Si II, Si IV, C IV, Fe II, Al II	1, 2, 3
				3.995	20.15±0.10	O I, C II, Si IV, C IV, Fe II	3
PSS0134+3307	4.536	2.976	4.481	3.760	20.60±0.10	Si II, Si IV, C IV, Al II	1, 2
PSS0209+0517	4.194	2.943	4.142	3.666	20.50±0.10	Si II, Fe II, Al II	1, 2, 3
				3.862	20.30±0.15	O I, C II, Si II, Al II	1, 2, 3
				3.139	20.05±0.25	Si II, C IV, Fe II, Al II	
PSS0211+1107	3.975	2.847	3.925	3.502	20.10±0.20	Si II, C IV, Fe II, Al II	
PSS0747+4434	4.435	3.107	4.381	3.762	20.00±0.20	no metals ^d	1, 2
				4.019	21.10±0.15	O I, C II, Si II, Fe II, Al II	1, 2, 5
				3.472	19.90±0.07	Fe II, Al II	
PSS0950+5801	3.973	2.759	3.923	3.264	20.50±0.10	Si III, Si II, C IV, Fe II, Al II	4, 5
BR0951-0450	4.35	2.866	4.296	3.235	20.25±0.10	C IV, Fe II, Al II	
				3.856	20.70±0.20	Si II, Si IV, C IV, Al II	2
				4.202	20.35±0.15	Si II, O I, C IV	2
PSS0955+5940	4.34	3.070	4.287	3.542	20.30±0.10	Si II, C IV, Fe II, Al II	4, 5
				3.843	20.00±0.15	Si IV, Si II, C IV, Al II	4, 5
				4.044	20.10±0.15	O I, C II, Si II, Si IV, C IV	
PSS0957+3308	4.283	2.969	4.230	3.043	19.65±0.15	C II, Al II	
				3.280	20.50±0.10	Fe II, Al II	
				3.364	19.70±0.15	Al II	
				3.900	19.50±0.10	no metals	
				4.179	20.60±0.10	O I, C II, Si II, Si IV, C IV	
BRI1013+0035	4.38	3.123	4.326	3.738	20.15±0.20	no metals	
PSS1026+3828	4.18	2.756	4.128	3.339	19.72±0.08	no metals over available coverage ^c	
				3.865	19.90±0.10	C II	
PSS1039+3445	4.39	2.881	4.336	4.098	19.65±0.10	O I, C II, Si I V	
PSS1057+4555	4.126	2.776	4.075	2.909	20.05±0.10	Fe II, Al II	1, 2
				3.058	19.80±0.15	C IV, Fe II, Al II	1, 2
				3.164	19.50±0.20	Si II, C IV, Fe II, Al II	
				3.317	20.15±0.10	Si II, Fe II, Al II	1, 2
PSS1058+1245	4.330	3.110	4.277	3.430	20.40±0.15	no metals over available coverage ^c	
PSS1118+3702	4.03	2.893	3.980	3.698	19.87±0.08	O I, C II, Si II, Al II	
PSS1159+1337	4.081	2.823	4.030	3.726	20.00±0.10	C II, Si II, Si IV, C IV	1, 2
PSS1247+3406	4.897	3.314	4.838	4.572	19.80±0.10	Si IV, C IV	
PSS1248+3110	4.346	3.088	4.293	3.697	20.35±0.10	Si II, Fe II, Al II	
				4.075	20.20±0.15	O I, C II, Si IV	
				3.723	19.50±0.20	C IV	1, 2
PSS1253-0228	4.007	2.868	3.957	3.608	19.95±0.10	C II, Si IV, C IV, Fe II	
PSS1317+3531	4.369	2.998	4.315	3.461	19.90±0.05	Si II, C IV, Fe II, Al II	
J1325+1123	4.400	3.017	4.346	3.723	19.50±0.20	C IV	

Table 2. continued.

QSO	z_{em}	z_{min}	z_{max}	DLA-subDLA		Metal Lines	Note [*]
				z_{abs}	$\log N(\text{H I})$		
PSS1326+0743	4.123	2.866	4.072	4.133	19.50±0.20	no metals ^b	
				2.919	19.95±0.10	Al II	
				3.425	19.90±0.15	Al II	
PSS1432+3940	4.292	3.105	4.239	3.274	21.00±0.15	C IV, Fe II, Al II	
PSS1435+3057	4.35	2.942	4.297	3.267	20.05±0.10	C IV, Al II	
				3.516	20.20±0.10	Si II, C IV, Al II	
				3.778	19.85±0.10	C IV, Al II	
PSS1443+2724	4.406	3.095	4.352	4.223	20.90±0.15	Si IV, Si II, C IV, Fe II, Al II	2
PSS1500+5829	4.224	3.031	4.172	3.585	19.55±0.10	no metals over available coverage ^c	
				3.915	20.50±0.10	O I	
PSS1506+5220	4.18	3.275	4.128	3.223	20.70±0.10	Si II, C IV, Fe II, Al II, Al III	
PSS1531+4157	4.20	2.868	4.148	3.657	19.55±0.15	Si II, C IV, Al II	
PSS1535+2943	3.972	2.797	3.922	3.202	20.60±0.10	Si II, C IV, Fe II, Al II	
				3.762	20.55±0.15	O I, C II, Si IV, C IV, Al II	
PSS1554+1835	3.99	2.769	3.940	2.919	20.00±0.15	Si II, C IV, Al II, Al III	
PSS1555+2003	4.228	2.824	4.176	3.427	19.90±0.10	no metals over available coverage ^c	
PSS1633+1411	4.349	2.836	4.296	2.880	20.30±0.15	Fe II, Si II	
PSS1646+5514	4.084	2.800	4.033	2.932	19.50±0.10	no metals over available coverage ^c	
				4.029	19.80±0.15	no metals over available coverage ^c	
PSS1715+3809	4.52	3.004	4.465	3.341	21.05±0.20	Si II, Fe II, Al II	
PSS1723+2243	4.515	3.062	4.460	3.697	20.35±0.10	Si II, C IV, Fe II, Al II	
SDSS1737+5828	4.94	3.383	4.881	4.152	19.85±0.15	Si II, Al II	
				4.741	20.65±0.15	Si II, O I, C II	4, 5
PSS1745+6846	4.13	2.860	4.079	3.706	19.73±0.09	Si II, C IV, Al III	
PSS1802+5616	4.158	2.821	4.106	3.391	20.25±0.10	Si IV, Si II, C IV, Fe II, Al II	1, 2
				3.554	20.40±0.10	O I, Si II, C IV, Fe II, Al II	1, 2
				3.762	20.65±0.15	C II, Si II, Fe II, Al II	1, 2
				3.811	20.35±0.15	C II, Si IV, Si II, Al II	1, 2
PSS2122-0014	4.114	2.903	4.063	3.207	20.20±0.10	Si II, C IV, Fe II, Al II	1, 2, 4, 5
				3.264	19.90±0.15	C IV, Al II	
				4.001	20.15±0.15	C II, Si IV, C IV	1, 2
PSS2155+1358	4.256	3.064	4.203	3.143	19.90±0.20	Fe II, Al II	
				3.318	20.75±0.20	Si II, Fe II, Al II	1, 2
				4.211	20.00±0.10	Si II, O I, C II	
PSS2203+1824	4.375	2.850	4.321	3.610	19.70±0.15	Si II, C IV, Al II	
				4.107	19.80±0.15	C II, Si II, Fe II, Al II	
PSS2238+2603	4.031	2.816	3.981	3.857	20.45±0.15	Si II, O I, C II, Si IV, C IV, Fe II, Al II	
PSS2241+1352	4.441	3.106	4.387	3.656	20.15±0.20	Al II, Si II	1, 2
				4.281	20.75±0.15	Si II, O I, C II, Fe II, Al II	1, 2, 4, 5
PSS2315+0921	4.412	2.863	4.358	3.220	21.25±0.15	C II, Si II, Fe II, Al II	
				3.425	21.00±0.20	Si II, C IV, Fe II, Al II	
PSS2322+1944	4.17	2.754	4.118	2.888	19.95±0.10	Fe II, Al II	
				2.975	19.80±0.10	Fe II, Al II	
PSS2323+2758	4.18	2.823	4.128	2.952	19.80±0.10	no metals	
				3.684	20.60±0.15	Si II, Fe II	
PSS2344+0342	4.340	2.939	4.287	3.220	21.20±0.10	no metals over available coverage ^{c,d}	1, 2
				3.884	19.80±0.10	no metals over available coverage ^{c,e}	

^a Metals were detected by Péroux et al. (2005)^b Metals were detected by Prochaska & Wolfe (2009)^c We do not cover the red part of the spectrum $\lambda \geq 6400 \text{ \AA}$ ^d Metals were detected by Péroux et al. (2001)^e Metals were detected by Dessauges-Zavadsky et al. (2003)^{*} The same references that appears in Table 1

Table 3. QSOs without detected DLAs and/or sub-DLAs

QSO	z_{em}	z_{min}	z_{max}	Note*
PSS0014+3032	4.470	2.866	4.415	
SDSS0210-0018	4.700	3.177	4.643	4, 5
PSS0248+1802	4.430	3.118	4.376	2
PSS0452+0355	4.395	3.115	4.341	
PSS0852+5045	4.216	2.939	4.164	
PSS0926+3055	4.198	2.951	4.146	
SDSS0941+5947	4.820	3.322	4.762	4, 5
PSS1140+6205	4.509	3.113	4.454	4, 5
SDSS1310-0055	4.152	2.830	4.101	4, 5
PSS1339+5154	4.080	2.783	4.029	5
PSS1401+4111	4.026	2.866	3.976	4, 5
PSS1403+4126	3.862	2.866	3.813	4, 5
PSS1418+4449	4.323	2.974	4.270	4, 5
PSS1430+2828	4.306	2.811	4.253	2
PSS1458+6813	4.291	2.990	4.238	
GB1508+5714	4.304	3.217	4.251	2
PSS1543+3417	4.407	3.071	4.353	5
PSS1615+1803	4.010	2.783	3.960	
PSS1721+3256	4.040	2.802	3.990	1, 2
PSS2154+0335	4.359	3.400	4.305	1, 2, 3
PSS2244+1005	4.040	2.810	3.990	

* Quasars from this survey were previously used for $\Omega_{\text{DLA}, \text{H}_1}$ estimations by: (1) Péroux et al. (2001); (2) Péroux et al. (2003); (3) Péroux et al. (2005); (4) Prochaska et al. (2005); Prochaska & Wolfe (2009)

Table 4. Principal absorption metal lines most frequently detected associated to high column density absorption systems.

Ion	λ_0 (Å)	f^a	$\log \lambda_0 f + \log [N/N(H)]_\odot + 12.00$
Si III	1206.500	0.221	10.87
H I	1215.6701	0.4162	14.70
N V	1238.821	0.152	10.24
N V	1242.804	0.0757	9.93
Si II	1260.4223	0.959	10.65
O I	1302.1685	0.0486	10.67
Si II	1304.3702	0.147	9.85
C II	1334.5323	0.118	10.85
Si IV	1393.76018	0.528	10.44
Si IV	1402.770	0.262	10.13
Si II	1526.70698	0.23	10.11
C IV	1548.2041	0.194	11.13
C IV	1550.7812	0.097	10.83
Fe II	1608.45085	0.062	9.52
Al II	1670.7886	1.88	9.99
Al III	1854.7164	0.539	9.49
Al III	1862.7895	0.268	9.19
Fe II	2344.2139	0.108	9.92
Fe II	2374.4162	0.0395	9.49
Fe II	2382.7652	0.328	10.41

^a Oscillator strengths taken from Morton (1991).

Table 5. Frequency distribution fitting parameters

Form	z_{range}	$\log K$	α	$\log N_T$	β
Power-Law	[2.55 - 5.03]	6.59 \pm 2.12	-1.384 \pm 0.105	—	—
	[2.55 - 3.40]	5.55 \pm 2.88	-1.330 \pm 0.144	—	—
	[3.40 - 3.83]	4.03 \pm 2.01	-1.056 \pm 0.199	—	—
	[3.83 - 5.03]	4.38 \pm 2.39	-1.279 \pm 0.118	—	—
Double Power-Law	[2.55 - 5.03]	-21.78 \pm 0.31	-1.162 \pm 0.118	20.60 \pm 0.24	-2.07 \pm 0.51
	[2.55 - 3.40]	-22.64 \pm 1.25	-1.327 \pm 0.307	21.19 \pm 1.44	-5.98 \pm 2.07
	[3.40 - 3.83]	-21.28 \pm 0.19	-0.793 \pm 0.233	20.45 \pm 0.14	-2.49 \pm 0.74
	[3.83 - 5.03]	-21.63 \pm 0.25	-0.920 \pm 0.199	20.51 \pm 0.17	-2.10 \pm 0.44
Gamma	[2.55 - 5.03]	-21.95 \pm 0.36	-1.010 \pm 0.172	20.93 \pm 0.18	—
	[2.55 - 3.40]	-22.53 \pm 1.54	-1.185 \pm 0.329	21.28 \pm 0.89	—
	[3.40 - 3.83]	-20.96 \pm 0.28	-0.485 \pm 0.324	20.45 \pm 0.16	—
	[3.83 - 5.03]	-21.80 \pm 0.35	-0.853 \pm 0.198	20.82 \pm 0.18	—

Table 6. Absorption Distance Path - Data for Figure 8

z_{range}	$< z >$	N_{QSO}	N_{DLA}	N_{subDLA}	ΔX	$\Omega_{\text{DLA}}(10^3)$	$\Omega_{\text{DLA+subDLA}}(10^3)$
2.55 - 3.40	3.168	77	12	23	125.922	1.43 \pm 0.33	1.71 \pm 0.33
3.40 - 3.83	3.618	78	17	19	125.922	1.41 \pm 0.26	1.65 \pm 0.26
3.83 - 5.03	4.048	77	11	18	125.922	0.97 \pm 0.22	1.21 \pm 0.22

Appendix : Notes on individual systems

In this Appendix we discuss systems where we note differences between our measurements and measurements by others.

1. PSS 0131+0633 ($z_{\text{em}} = 4.430$). Péroux et al. (2001) report two sub-DLA candidates at $z_{\text{abs}} = 3.17$ and 3.61 with $\log N(\text{H I}) = 19.9$ and 19.8 respectively. For the second system however, Péroux et al. (2001) give in Table 5 a redshift of $z_{\text{abs}} = 3.61$ for the H I line and $z_{\text{abs}} = 3.609$ for the metal lines but a redshift of $z_{\text{abs}} = 3.69$ and $\log N(\text{H I}) = 19.5$ in their Section 8 namely, "Notes on Individual Objects". We also detect the first sub-DLA at $z_{\text{abs}} = 3.173$ with $\log N(\text{H I}) = 19.95 \pm 0.10$. Metal lines at that redshift are detected in the red part of the spectrum. For the second DLA candidate, we confirm the presence of the $z_{\text{abs}} = 3.689$ absorption with $\log N(\text{H I}) = 19.50 \pm 0.10$ in agreement with the sub-DLA candidate reported in Section 8 of Péroux et al. (2001). Metal lines at that redshift are also observed in the red part of the spectrum.
2. PSS0747+4434 ($z_{\text{em}} = 4.435$). Péroux et al. (2001) report two DLA candidates at $z_{\text{rmabs}} = 3.76$ and 4.02 with $\log N(\text{H I}) = 20.3$ and 20.6 respectively, which are confirmed by our observations. We measure $\log N(\text{H I}) = 20.00 \pm 0.20$ at $z_{\text{abs}} = 3.762$ and $\log N(\text{H I}) = 21.10 \pm 0.15$ at $z_{\text{abs}} = 4.019$. No metal lines at $z_{\text{abs}} = 3.76$ are observed in both surveys. We remind the reader that our data are of higher spectral resolution.
3. SDSS 0756+4104 ($z_{\text{em}} = 5.09$). We detect a sub-DLA candidate at $z_{\text{abs}} = 4.360$ with $\log N(\text{H I}) = 20.15 \pm 0.10$. Although no Lyman series and metals are detected for this system, the spectrum has a high enough SNR to fit the H I line well and to ascertain that this absorber is highly likely to be Damped.
4. BR 0951–450 ($z_{\text{em}} = 4.35$). PMSI03 report the detection of two DLA candidates at $z_{\text{abs}} = 3.8580$ and 4.2028 with $\log N(\text{H I}) = 20.6$ and 20.4 respectively, which are confirmed by our observations. We measure $\log N(\text{H I}) = 20.70 \pm 0.20$ at $z_{\text{abs}} = 3.856$ and $\log N(\text{H I}) = 20.35 \pm 0.15$ at $z_{\text{abs}} = 4.202$. We discover an additional Damped candidate at $z_{\text{abs}} = 3.235$ with $\log N(\text{H I}) = 20.25 \pm 0.10$. We believe that this system is not included in the statistical sample of PMSI03, because it falls below the threshold of $\log N(\text{H I}) = 20.30$. Metal lines at that redshift are observed in the red part of the spectrum.
5. BRI 1013+0035 ($z_{\text{em}} = 4.38$). PMSI03 report one DLA candidate at $z_{\text{abs}} = 3.103$ with $\log N(\text{H I}) = 21.1$. This system is not included in our sample since its redshift is smaller than the minimum redshift beyond which a DLA/sub-DLA could be detected in our spectrum. One Damped candidate was discovered at $z_{\text{abs}} = 3.738$ with $\log N(\text{H I}) = 20.15 \pm 0.20$. We believe that this system is not included in the statistical sample of PMSI03 because it falls below the threshold of $\log N(\text{H I}) = 20.30$. Although no lyman series and metals are detected for this system, the SNR in the spectrum is high enough to ascertain that this absorber is highly likely to be Damped.
6. PSS 1057+4555 ($z_{\text{em}} = 4.126$). Péroux et al. (2001) report three DLA candidates at $z_{\text{abs}} = 2.90$, 3.05 and 3.32 with $\log N(\text{H I}) = 20.1$, 20.3 and 20.2 respectively, which are confirmed by our observations. We measure $\log N(\text{H I}) = 20.05 \pm 0.10$ at $z_{\text{abs}} = 2.909$, $\log N(\text{H I}) = 19.80 \pm 0.15$ at $z_{\text{abs}} = 3.058$ and $\log N(\text{H I}) = 20.15 \pm 0.10$ at $z_{\text{abs}} = 3.317$. Metal lines at all three redshifts are observed in the red part of the spectrum. We report a new sub-DLA at $z_{\text{abs}} = 3.164$ with $\log N(\text{H I}) = 19.50 \pm 0.20$. Several metal lines are detected for this system.
7. PSS 1253–0228 ($z_{\text{em}} = 4.007$). Péroux et al. (2001) report two DLA candidates at $z_{\text{abs}} = 2.78$ and 3.60 with $\log N(\text{H I}) = 21.4$ and 19.7 , respectively. The system at $z_{\text{abs}} = 2.78$ is not included in our sample because its redshift falls below the minimum redshift beyond which DLA/sub-DLA could be detected in our spectrum. We measure $\log N(\text{H I}) = 19.95 \pm 0.10$ at $z_{\text{abs}} = 3.608$. Several metal lines are detected for this system.
8. J 1325+1123 ($z_{\text{em}} = 4.400$). We have discovered two sub-DLA candidates at $z_{\text{abs}} = 3.723$ and 4.133 with $\log N(\text{H I}) = 19.50 \pm 0.20$ and 19.50 ± 0.20 , respectively. C IV metal lines are detected at $z_{\text{abs}} = 3.723$. This two sub-DLAs can be found in the list of SDSS DR5 systems available on Jason Prochaska's website.
9. PSS 1633+1411 ($z_{\text{mem}} = 4.349$). Péroux et al. (2001) report one sub-DLA candidate at $z_{\text{abs}} = 3.90$ with $\log N(\text{H I}) = 19.8$. Here, we measure $\log N(\text{H I}) = 19.0 \pm 0.20$ at $z_{\text{abs}} = 3.909$. We report a new DLA at $z_{\text{abs}} = 2.880$ with $\log N(\text{H I}) = 20.30 \pm 0.15$. Several metal lines are detected for this system.
10. PSS 1646+5514 ($z_{\text{em}} = 4.084$). No DLA candidate is detected by Péroux et al. (2001) along this line of sight. We report here two sub-DLA candidates at $z_{\text{abs}} = 2.932$ and 4.029 with $\log N(\text{H I}) = 19.50 \pm 0.10$ and 19.80 ± 0.15 , respectively. No metals are seen over the available wavelength coverage.
11. PSS 2122–0014 ($z_{\text{em}} = 4.084$). Péroux et al. (2001) report two candidates at $z_{\text{abs}} = 3.20$ and 4.00 with $\log N(\text{H I}) = 20.3$ and 20.1 , respectively. Here, we measure $\log N(\text{H I}) = 20.20 \pm 0.10$ and 20.15 ± 0.15 at $z_{\text{abs}} = 3.207$ and 4.001 . Several metal lines are detected for both systems. We report a new sub-DLA candidate at $z_{\text{abs}} = 3.264$ with $\log N(\text{H I}) = 19.90 \pm 0.15$. Several metal lines are detected also for this system.
12. PSS 2154+0335 ($z_{\text{em}} = 4.359$). Péroux et al. (2001) report two candidates at $z_{\text{abs}} = 3.61$ and 3.79 with $\log N(\text{H I}) = 20.4$ and 19.70 , respectively. No candidate with $\log N(\text{H I}) > 19.50$ is detected in our spectrum.
13. PSS 2155+1358 ($z_{\text{em}} = 4.256$). Péroux et al. (2001) report one DLA at $z_{\text{abs}} = 3.32$ with $\log N(\text{H I}) = 21.10$. Dessauges et al. (2003) report three sub-DLAs at $z_{\text{abs}} = 3.142$, 3.565 and 4.212 with $\log N(\text{H I}) = 19.94$, 19.37 and 19.61 . Here, we measure $\log N(\text{H I}) = 19.90 \pm 0.20$, 20.75 ± 0.20 and 20.00 ± 0.10 at $z_{\text{rmabs}} = 3.143$, 3.318 and 4.211 , respectively. Several metal lines are detected for these systems.
14. PSS2344+0342 ($z_{\text{em}} = 4.340$). Péroux et al. (2001) report two DLAs at $z_{\text{abs}} = 2.68$ and 3.21 with $\log N(\text{H I}) = 21.10$ and 20.9 . The first system is not included in our sample because its redshift falls below the minimum redshift beyond which a

DLA/sub-DLA could be detected in our spectrum. We measure $\log N(\text{H I}) = 21.20 \pm 0.10$ at $z_{\text{abs}} = 3.220$. Dessauges et al. (2003) report one sub-DLA at $z_{\text{abs}} = 3.882$ with $\log N(\text{H I}) = 19.50$. We measure $\log N(\text{H I}) = 19.80 \pm 0.10$ at $z_{\text{abs}} = 3.884$.

Appendix : List of Figures

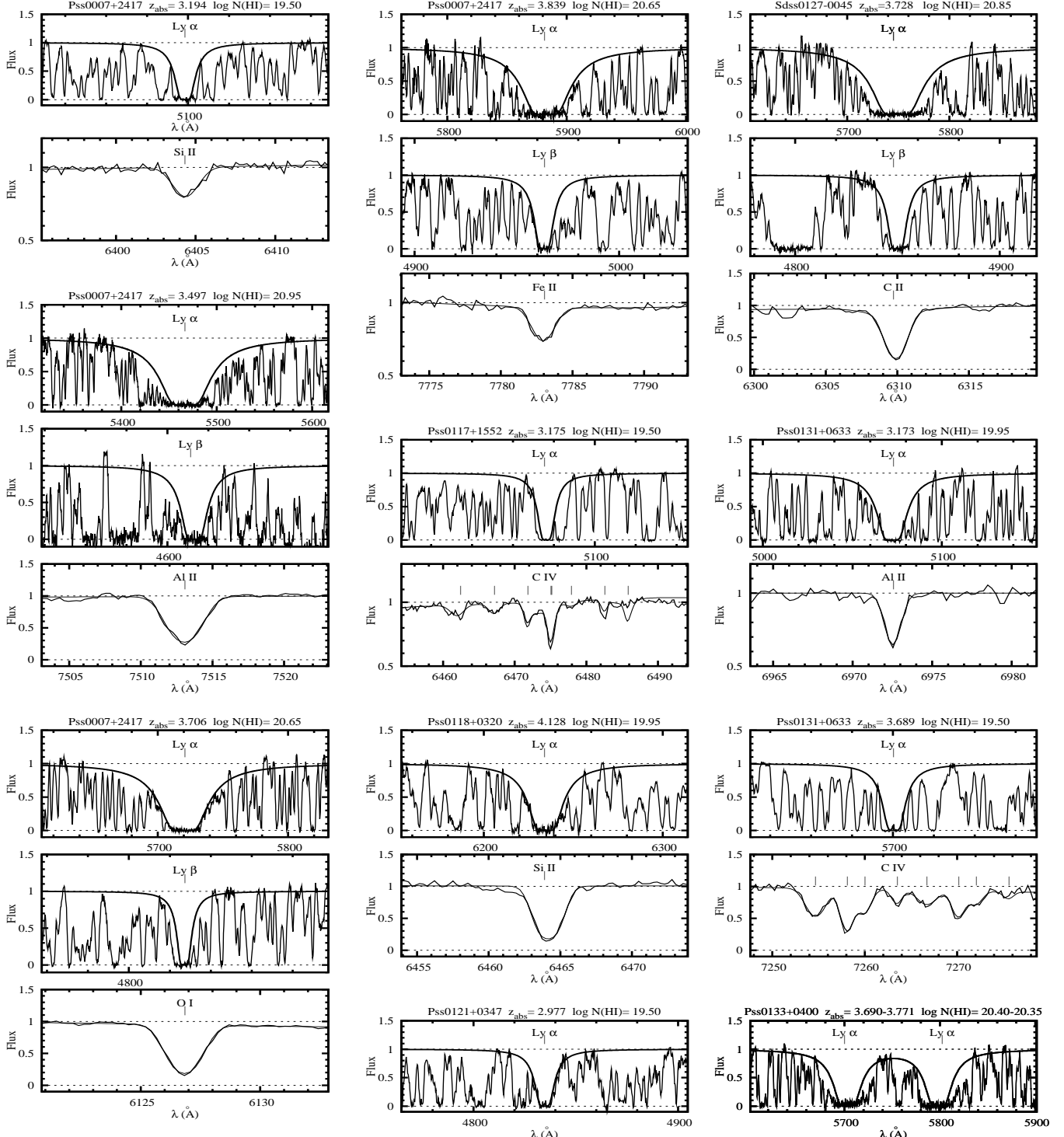


Fig. 1. Spectra of the 100 confirmed Lyman- α absorption with $\log N(\text{H I}) \geq 19.5$. In each panel the Voigt profile fit corresponding to the best $N(\text{H I})$ value is overplotted. The Lyman series absorption lines and one characteristic associated metal absorption feature (when metals are present over the available wavelength coverage and not blended with another lines) are presented in additional sub-panels.

